COMMUNICATION

High Iodine Uptake in Two-Dimensional Covalent Organic Frameworks

Received 00th January 20xx,
Accepted 00th January 20xx

DOI: 10.1039/x0xx00000x

Lingyan Zhang,[ac] Jinheng Li,[ac] Huixin Zhang,[a] Yu Liu,[ab] Yumeng Cui,[a] Fenchun Jin,[a] Ke Wang,[a] Guiyan Liu,*[a] Yanli Zhao*[b] and Yongfei Zeng*[a]

Two two-dimensional covalent organic frameworks (COFs, TJNU-203 and TJNU-204) with high crystallinity and large specific surface areas are rationally fabricated from a three-connected distorted building block and linear linkers. The two COFs show high iodine uptake (5.885 g/g for TJNU-203 and 5.335 g/g for TJNU-204) on account of the physical-chemical adsorption, which are among the best porous materials for iodine adsorption.

Radionuclide ^{129}I is the main radioactive waste from nuclear reactions, which is extremely harmful to human beings and nature.[1] To reduce pollution caused by radioactive iodine, some porous materials have been already developed for iodine capture, such as metal-organic frameworks (MOFs),[2] zeolites,[3] activated carbon,[4] porous organic polymers (POPs),[5] and supramolecular materials.[6] Covalent organic frameworks (COFs) have been also proposed as one of the ideal materials to relieve the nuclear waste crisis. COFs are an important type of crystalline organic porous materials with periodic structures connected by organic units through covalent bonds, which can be precisely predesigned by reticular chemistry.[7] Excellent properties such as large surface area, high porosity, good crystallinity, structural diversity, and easy functionalization enable COFs to present a wide range of applications.[8] In 2017, Zhao et al. reported a COF material (SIOC-COF-7) for iodine capture,[9] showing a high volatile iodine capture capacity (481 wt% (4.81 g/g)). Jiang and coworkers documented a series of COFs with good adsorption capacity for iodine by physical adsorption or physical-chemical adsorption.[10,11] Xia et al. also constructed two-dimensional (2D) COFs, where the crystallinity and volatile iodine adsorption performance were modulated by the content of hydrogen bonds in COFs. The COF without hydrogen bonds showed high iodine adsorption capacity (5.43 g/g)).[12] Ke et al. reported a crystalline microporous hydrogen-bonded COF, which possessed an iodine adsorption capacity (290 wt% (2.90 g/g)) in an aqueous environment.[13] Thomas and coworkers developed a Fe_3O_4/COF composite material that could capture iodine in iodine aqueous solution with adsorption capacity of 797 mg/g.[14]

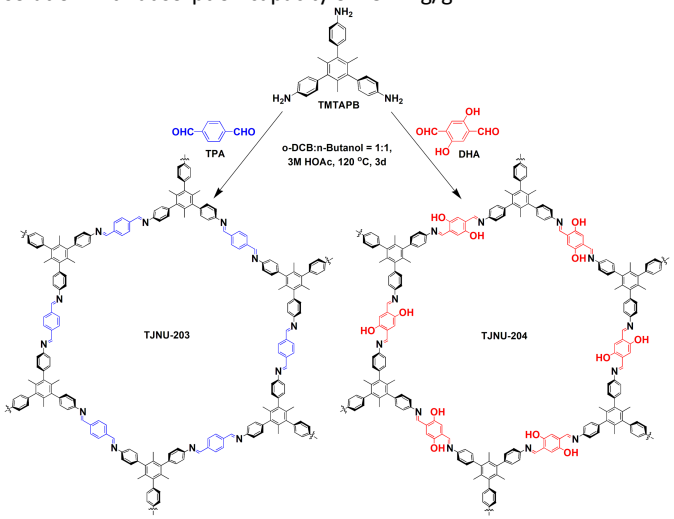

Scheme 1. Synthetic scheme of TJNU-203 and TJNU-204.

Although a great progress has been achieved, the pursuit of COFs with high iodine capture is still a great challenge. Recently, we reported a 2D COF (TJNU-201) based on a twisted three-connected unit (1,3,5-trimethyl-2,4,6-tris(4-aminophenyl)benzene, TMTAPB) and a planar triangular building block, showing a high iodine adsorption ability (5.625 g/g) due to the combination of chemisorption and physisorption.[15] To some extent, the incorporation of twisted TMTAB in TJNU-201 can efficiently expose the chemisorption site (*e.g.*, C=N group), which can readily interact with iodine molecule to increase the chemisorption capacity, thus obtaining a large total adsorption value. However, the relatively low density of chemisorption sites in TJNU-201 still restricted its capacity toward iodine adsorption. Therefore, we hypothesized that further increasing the density of chemical adsorption sites (*e.g.*, C=N group) may effectively improve the iodine adsorption capacity.

Herein, we designed and synthesized two novel 2D COFs (TJNU-203 and TJNU-204) from TMTAPB and linear dialdehyde organic units. Compared with TJNU-201, TJNU-203 and TJNU-204 not only expose more chemisorption sites, but also possess a one-dimensional (1D)

[a] *Tianjin Key Laboratory of Structure and Performance for Functional Molecules, Key Laboratory of Inorganic-Organic Hybrid Functional Material Chemistry (Ministry of Education), College of Chemistry, Tianjin Normal University, Tianjin, 300387 (P. R. China). E-mail: guiyanliu2013@163.com; yfzeng@nankai.edu.cn.*
[b] *Division of Chemistry and Biological Chemistry, School of Physical and Mathematical Sciences, Nanyang Technological University, 21 Nanyang Link, 637371 Singapore (Singapore). E-mail: zhaoyanli@ntu.edu.sg.*
[c] *These authors contributed equally to this work.*
† Electronic Supplementary Information (ESI) available: Synthesis and characterization details. See DOI: 10.1039/x0xx00000x

Please do not adjust margins

triangular pore channel. In particular, TJNU-203 and TJNU-204 present high iodine uptake values of 5.885 and 5.335 g/g due to efficient physical-chemical adsorption, making them one of the best porous materials for iodine capture.

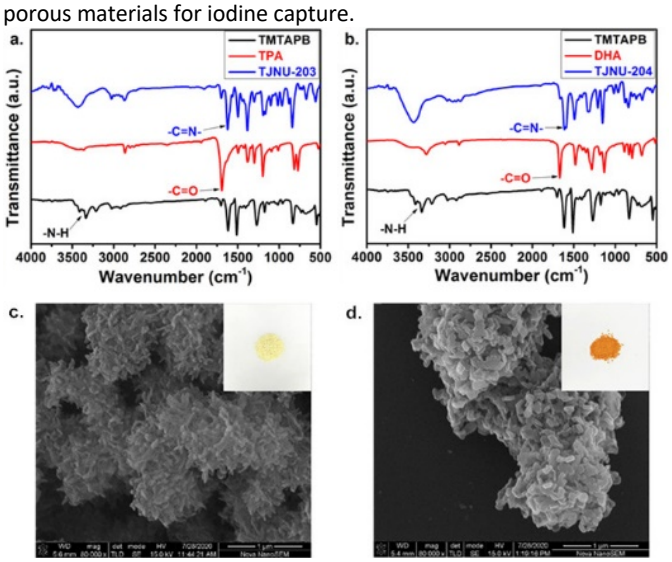

Figure 1. FT-IR spectra of (a) TJNU-203 and (b) TJNU-204. SEM images of (c) TJNU-203 and (d) TJNU-204.

TJNU-203 and TJNU-204 were constructed by the condensation reaction of TMTAPB and terephthalaldehyde (TPA) (or 2,5-dihydroxy-1,4-benzenedicarboxaldehyde (DHA)) in a mixed solvent (1,2-dichlorobenzene/n-butanol (v/v 1:1)) in the presence of 3M acetic acid aqueous solution at 120 °C for 3 days (Scheme 1). TJNU-203 and TJNU-204 were firstly characterized by Fourier-transform infrared (FTIR) spectroscopy. The vibration of C=N bond was observed at 1623 cm^{-1} for TJNU-203 and 1613 cm^{-1} for TJNU-204, implying the formation of imine bond (Figure 1a,b, S1 and S2). The formation of imine bond was further confirmed by solid-state ^{13}C nuclear magnetic resonance (NMR) spectroscopy. The characteristic signals at 157 and 163 ppm were attributed to the carbon atom of imine bond in TJNU-203 and TJNU-204, respectively (Figure S3 and S4). According to scanning electron microscope (SEM) images, TJNU-203 as a yellow powder is a flower-shape with a particle size of 0.25 µm, and TJNU-204 as an orange-red powder shows a flake morphology with a particle size of 0.21 µm (Figure 1c,d and S5). Both COFs exhibited high thermal stability (>450 °C) by thermogravimetric analysis (TGA) under a nitrogen atmosphere (Figure S6 and S7).

To assess the crystallinity of TJNU-203 and TJNU-204, their powder X-ray diffraction (PXRD) patterns were obtained (Figure 2). Both TJNU-203 and TJNU-204 showed good crystallinity. For TJNU-203, the diffraction peaks appear at 2θ = 4.63°, 5.40°, 7.03°, 9.27°, 11.70°, 15.05° and 20.22° (Figure S8), while 4.65°, 5.77°, 7.49°, 9.33° and 15.43° for TJNU-204 (Figure S9). The crystalline structures of TJNU-203 and TJNU-204 were analyzed by the PXRD profiles together with structural simulations (Figure 2 and S10-S17). After geometry optimizations, the 2D extended structures were modelled for TJNU-203 and TJNU-204. At first, the eclipsed (AA) and staggered (AB) stacking structures were proposed for TJNU-203 and TJNU-204 (Figure S11, S12, S15 and S16). Unfortunately, all the simulated patterns based on the eclipsed (AA) and staggered (AB) stacking structures cannot match their corresponding experimental PXRD patterns. Then, the ABC stacking architecture based on the space $R\bar{3}m$ (no. 166) was constructed for TJNU-203 and TJNU-204, affording the unit cell parameters of a = b = 38.127 Å and c = 17.300 Å for TJNU-203 and a = b = 38.012 Å and c = 19.030 Å for TJNU-204. Encouragingly, their simulated PXRD patterns are in good agreement with the experimental patterns in terms of both peak positions and relative intensities (Figure S13 and S17), indicating the validity of proposed structure. Finally, Pawley refinements were carried out, giving suitable agreement factors of wRp = 4.07%, Rp = 3.27% for TJNU-203 and wRp = 4.06%, Rp = 2.83% for TJNU-204 (Figure 2). Taking the above results into account, the obtained COFs should have a 2D framework with the ABC stacking structure, showing 1D microporous channels with the diameter of ~1.0 nm (Figure 2). Due to the steric hindrance of methyl groups, the peripheral phenyl groups of TMTAPB and the imine bonds of TPA or DHA unit arrange in a vertical manner to form the 2D sheets, thus highly exposing the aromatic rings and imine groups to the 1D pore channels for efficiently interacting with suitable guest molecules.

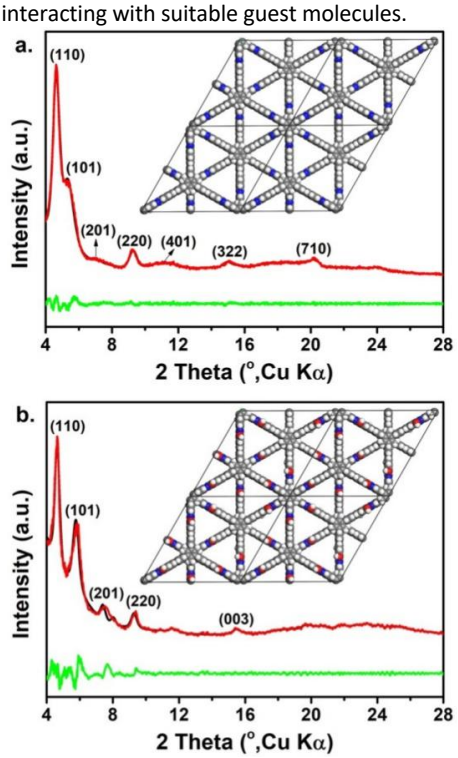

Figure 2. Experimental PXRD profile (red), Pawley refinement PXRD profile (black), and the differences between the experimental and refined PXRD patterns (green) of (a) TJNU-203 and (b) TJNU-204. Inset: the structure of ABC stacking mode for (a) TJNU-203 and (b) TJNU-204.

To evaluate the permanent porosity of TJNU-203 and TJNU-204, the N_2 adsorption/desorption measurements were carried out at 77 K. TJNU-203 and TJNU-204 exhibited classic type I isotherm curves, indicating the microporous feature (Figure S18 and S19). The Brunauer–Emmett–Teller (BET) surface areas of TJNU-203 and TJNU-204 were calculated from their N_2 adsorption/desorption isotherm data. The obtained BET surface areas are 1833 and 2048 m^2/g respectively (Figure S20 and S21), which are higher than that of some leading COFs such as TTA-TTB (1733 m^2/g),[10] COF-DL229 (1762 m^2/g)[11] and TJNU-202 (714 m^2/g).[15] The pore size distribution of

This journal is © The Royal Society of Chemistry 20xx

Please do not adjust margins

Please do not adjust margins

TJNU-203 and TJNU-204 was calculated by quenched solid density functional theory (QSDFT), giving the pore size of 0.98 and 0.89 nm, respectively (Figure S22 and S23). The pore size is consistent with the theoretical value (~1.0 nm), further confirming that TJNU-203 and TJNU-204 possess ABC stacking mode with the 1D triangular pore. Compared with the 1D hexagonal porous structures of TJNU-201 and TJNU-202 (similar to the reported TPB-DMTP COF[10]), TJNU-203 and TJNU-204 with the 1D triangular pore are analogue to the reported QTD-COF-V.[16] Additionally, TJNU-203 and TJNU-204 have smaller 1D pore than that of TJNU-201 (1.4 nm) and TJNU-202 (1.7 nm).[15]

Considering serious iodine pollution in nuclear waste, TJNU-203 and TJNU-204 were applied to the iodine vapor capture on account of their high porosity and rich active sites per unit size. In the iodine vapor capture experiments, the activated sample of TJNU-203 or TJNU-204 was exposed to iodine vapor in a chamber at 350 K under ambient pressure. From the iodine vapor adsorption curves (Figure 3a,b, S24 and S25), the iodine vapor adsorption rates for TJNU-203 and TJNU-204 remarkably increased within 48 h, after which their adsorption rates decreased gradually until the saturation. Interestingly, TJNU-203 showed an ultrahigh iodine absorption capacity of 5.885 g/g, which surpassed the reported porous materials (e.g., TTA-TTB,[10] COF-DL229,[11] TPT-BD COF,[12] and TJNU-201[15]) with the exception of TPB-DMTP (6.26 g/g),[10] QTD-COF-V (6.29 g/g),[16] and SCU-COF-2 (6.0 g/g).[17] The uptake capacity of TJNU-204 (5.335 g/g) was similar to that of TJNU-201[15] and TPT-BD COF[12] reported in literature. Notably, the uptake capacity of TJNU-203 and TJNU-204 is higher than other types of porous materials, such as MOFs,[2] zeolite,[3] activated carbon[4] and POPs.[5]

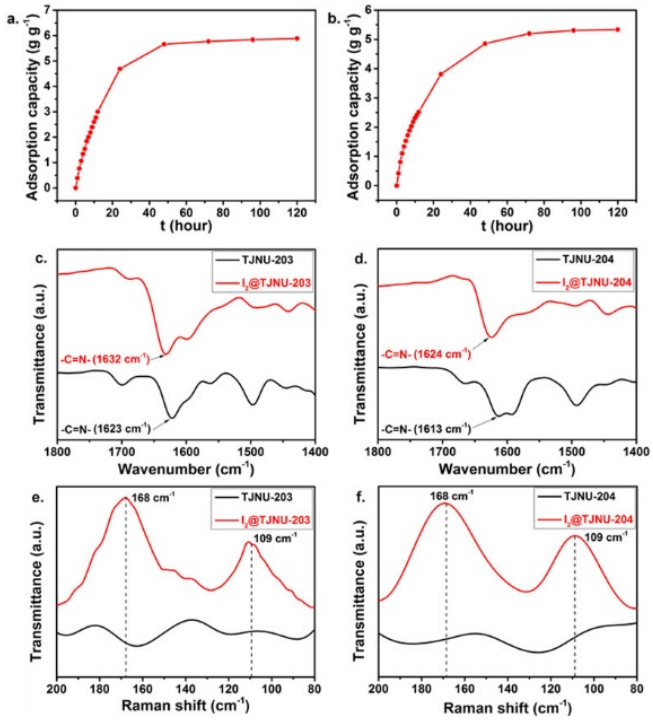

Figure 3. Gravimetric uptake of I_2 vapor by (a) TJNU-203 and (b) TJNU-204 as a function of time at 77 ºC and ambient pressure. FT-IR spectra of (c) TJNU-203 and I_2@TJNU-203 as well as (d) TJNU-204 and I_2@TJNU-204. Raman spectra of (e) TJNU-203 and I_2@TJNU-203 as well as (f) TJNU-204 and I_2@TJNU-204.

Furthermore, the iodine-loaded COFs (I_2@TJNU-203 and I_2@TJNU-204) were characterized by FTIR spectroscopy. The stretching vibration peak of the C=N bond presents an obvious blue shift from 1623 cm^{-1} to 1632 cm^{-1} for TJNU-203 (Figure 3c and S26) and from 1613 cm^{-1} to 1624 cm^{-1} for TJNU-204 (Figure 3d and S27), indicating the strong interactions between adsorbed iodine and the imine bonds of COFs for a chemisorption process.[15] Moreover, Raman spectroscopy of I_2@TJNU-203 and I_2@TJNU-204 was conducted. Compared with TJNU-203 and TJNU-204, I_2@TJNU-203 and I_2@TJNU-204 showed peaks at 109 and 168 cm^{-1}, which can be assigned to the stretching vibrations of I_3^- and I_5^- anions (Figure 3e,f). The generation of polyiodide ions confirmed the existence of chemical adsorption.[11-13,15,18] In order to further illustrate the existence of iodine, the COFs after iodine adsorption were analyzed by X-ray photoelectron spectroscopy (Figure S28 and S29). For I_2@TJNU-203 and I_2@TJNU-204, the splitting peaks at 629.4 eV and 619.7 eV respectively corresponding to the $I3d_{3/2}$ and $I3d_{5/2}$ orbitals[18] indicate that there are two types of iodine after the adsorption. Meanwhile, two absorption peaks appear at 631.2 eV and 617.9 eV, due to the interaction between iodine and aromatic rings. When compared I_2@TJNU-203 and I_2@TJNU-204 with TJNU-203 and TJNU-204, the N1s peak also shows obvious changes, further indicating the interaction between the imine bond and iodine.

The iodine release experiments were then carried out in methanol solution, which were monitored by UV/vis spectroscopy. Within the first 6 minutes, iodine was released rapidly and then the release became slowly (Figure 4). After 50 minutes, the iodine releasing content of I_2@TJNU-203 and I_2@TJNU-204 was about 68 wt%, and 66 wt% respectively, corroborating the existence of physical adsorption.[10,11,15] The iodine release rate and amount of I_2@TJNU-203 and I_2@TJNU-204 are equivalent to those of I_2@TJNU-201 and I_2@TJNU-202 (67.4 wt% and 63.2 wt% released within 50 minutes),[15] and higher than that of I_2@COF-DL229 (45 wt% released in 120 minutes).[11]

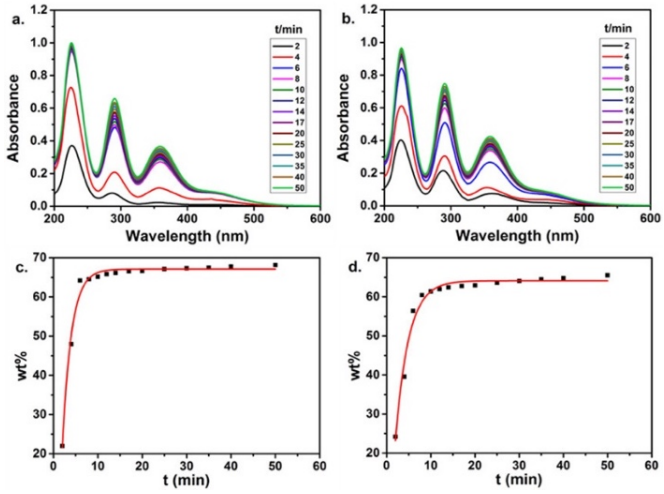

Figure 4. UV/vis spectra of iodine release from (a) I_2@TJNU-203 and (b) I_2@TJNU-204 in 50 minutes. Time-dependent iodine release curves from (c) I_2@TJNU-203 and (d) I_2@TJNU-204 into methanol in 50 minutes.

The adsorption mechanism of I_2 on COFs was studied by molecular simulations. The optimized configurations of adsorbed I_2 are shown in Figure S30. On both of TJNU-203 and TJNU-204, I_2 prefers to locate

Please do not adjust margins

Please do not adjust margins

close to the C=N bond, forming the I-N bond with the lengths of 2.93 and 2.99 Å respectively, due to the interaction between unsaturated bond and electrons of I_2. In addition, I_2 can also locate at the middle space of two aromatic rings that form a strong potential well for I_2 (Figure S31). When I_2 is adsorbed on the C=N group, the adsorption enthalpy calculated is 67.75 KJ/mol for TJNU-203 and 62.09 KJ/mol for TJNU-204. When I_2 is trapped in the middle of aromatic rings, the adsorption enthalpy is 48.41 KJ/mol for TJNU-203 and 64.11 KJ/mol for TJNU-204. Due to the steric hindrance of methyl groups, the peripheral phenyl groups of TMTAPB and the imine bonds of TPA or DHA unit arrange in a vertical manner to form the 2D sheets, thus exposing the aromatic rings and imine groups to the 1D pore channels and enlarging the distance of packed layers to form the free space for I_2 molecule. These factors enhance the I_2 adsorption capacity when compared with TJNU-201.

In addition, the recycling capability of TJNU-203 and TJNU-204 for iodine adsorption was evaluated by cycling experiments. The regenerated TJNU-203 and TJNU-204 obtained by heating the I_2@TJNU-203 and I_2@TJNU-204 samples at 423 K under vacuum can still reveal the uptake of 4.162 g/g and 2.876 g/g after five cycles respectively, indicating their good recyclability (Figure S32 and S33). Meanwhile, the PXRD patterns of recovered TJNU-203 and TJNU-204 after five cycles showed partial crystallinity loss (Figure S34 and S35), similar to previous reports.[11,12]

In conclusion, two novel 2D COFs with ABC stacking have been constructed from sterically hindered three-connected building block TMTAPB and linear linkers. These two COFs have high permanent porosity and 1D triangular pore channels with an average diameter of ~0.95 nm. The steric nature of TMTAPB makes the aromatic rings, imine groups and linear linkers exposed in the pore channels, showing much richer density of active sites for effective interactions with suitable guest molecules. Thus, the two COFs have shown ultrahigh iodine adsorption capacity (5.885 g/g for TJNU-203 and 5.335 g/g for TJNU-204) on account of physical-chemical adsorption. This strategy to increase the density of active sites improves the iodine adsorption capacity, which sheds light on the future design of advanced porous materials.

Acknowledgements

This work was supported by the National Natural Science Foundation of China (21771138) and the Ministry of Education Singapore under the Academic Research Funds (MOE-MOET2EP10120-0003).

Conflicts of interest

There are no conflicts to declare.

Notes and references

1 D. R. Haefner and T. J. Tranter, *Idaho National Laboratory*, **2007**.
2 (a) D. F. Sava, M. A. Rodriguez, K. W. Chapman, P. J. Chupas, J. A. Greathouse, P. S. Crozier and T. M. Nenoff, *J. Am. Chem. Soc.*, 2011, **133**, 12398-12401; (b) D. F. Sava, K. W. Chapman, M. A. Rodriguez, J. A. Greathouse, P. S. Crozier, H. Zhao, P. J. Chupas and T. M. Nenoff, *Chem. Mater.*, 2013, **25**, 2591-2596; (c) X. Zhang, I. d. Silva, H. G. W. Godfrey, S. K. Callear, S. A. Sapchenko, Y. Cheng, I. Vitórica-Yrezábal, M. D. Frogley, G. Cinque, C. C. Tang, C. Giacobbe, C. Dejoie, S. Rudić, A. J. Ramirez-Cuesta, M. A. Denecke, S. Yang and M. Schröder, *J. Am. Chem. Soc.*, 2017, **139**, 16289-16296; (d) G. Brunet, D. A. Safin, M. Z. Aghaji, K. Robeyns, I. Korobkov, T. K. Woo and M. Murugesu, *Chem. Sci.*, 2017, **8**, 3171-3177; (e) Y. Tang, H. Huang, J. Li, W. Xue and C. Zhong, *J. Mater. Chem. A*, 2019, **7**, 18324-18329; (f) Q. Zhao, L. Zhu, G. Lin, G. Chen, B. Liu, L. Zhang, T. Duan and J. Lei, *ACS Appl. Mater. Interfaces*, 2019, **11**, 42635-42645; (g) P. Chen, X. He, M. Pang, X. Dong, S. Zhao and W. Zhang, *ACS Appl. Mater. Interfaces*, 2020, **12**, 20429-20439; (h) L. Chen, J. Qian, D.-D. Zhu, S. Yang, J. Lin, M.-Y. He, Z.-H. Zhang and Q. Chen, *ACS Appl. Nano Mater.*, 2020, **3**, 5390-5398.
3 (a) K. W. Chapman, P. J. Chupas and T. M. Nenoff, *J. Am. Chem. Soc.*, 2010, **132**, 8897-8899; (b) A. Al-Mamoori, M. Alsalbokh, S. Lawson, A. A. Rownaghi and F. Rezaei, *Chem. Eng. J.*, 2020, **391**, 123583.
4 T. C. T. Pham, S. Docao, I. C. Hwang, M. K. Song, D. Y. Choi, D. Moon, P. Oleynikov and K. B. Yoon, *Energy Environ. Sci.*, 2016, **9**, 1050-1062.
5 (a) C. Pei, T. Ben, S. Xu and S. Qiu, *J. Mater. Chem. A*, 2014, **2**, 7179-7187; (b) Y. Chen, H. Sun, R. Yang, T. Wang, C. Pei, Z. Xiang, Z. Zhu, W. Liang, A. Li and W. Deng, *J. Mater. Chem. A*, 2015, **3**, 87-91; (c) Z. Yan, Y. Yuan, Y. Tian, D. Zhang and G. Zhu, *Angew. Chem. Int. Ed.*, 2015, **54**, 12733-12737; (d) A. Trabolsi, G. Das, T. Prakasam, S. Nuryyeva, D. S. Han, A. Abdel-Wahab, J. Olsen, K. Polychronopoulou, C. Platas-Iglesias, M. Jouiad and F. Ravaux, *J. Mater. Chem. A*, 2016, **4**, 15361-15369; (e) T. Geng, Z. Zhu, W. Zhang and Y. Wang, *J. Mater. Chem. A*, 2017, **5**, 7612-7617; (f) Y. Zhu, Y. Ji, D. Wang, Y. Zhang, H. Tang, X. Jia, M. Song, G. Yu and G. Kuang, *J. Mater. Chem. A*, 2017, **5**, 6622-6629; (g) T. Geng, S. Ye, Z. Zhu and W. Zhang, *J. Mater. Chem. A*, 2018, **6**, 2808-2816; (h) Y. Wang, J. Tao, S. Xiong, P. Lu, J. Tang, J. He, M. U. Javaid, C. Pan and G. Yu, *Chem. Eng. J.*, 2020, **380**, 122420.
6 B. Li, B. Wang, X. Huang, L. Dai, L. Cui, J. Li, X. Jia and C. Li, *Angew. Chem. Int. Ed.*, 2019, **58**, 3885-3889.
7 A. P. Côté, A. I. Benin, N. W. Ockwig, M. O'Keeffe, A. J. Matzger and O. M. Yaghi, *Science*, 2005, **310**, 1166-1170.
8 S. Karak, K. Dey, A. Torris, A. Halder, S. Bera, F. Kanheerampockil and R. Banerjee, *J. Am. Chem. Soc.*, 2019, **141**, 7572-7581.
9 Z. Yin, S. Xu, T. Zhan, Q. Qi, Z. Wu and X. Zhao, *Chem. Commun.*, 2017, **53**, 7266-7269.
10 P. Wang, Q. Xu, Z. Li, W. Jiang, Q. Jiang and D. Jiang, *Adv. Mater.*, 2018, **30**, 1801991.
11 C. Wang, Y. Wang, R. Ge, X. Song, X. Xing, Q. Jiang, H. Lu, C. Hao, X. Guo, Y. Gao and D. Jiang, *Chem. Eur. J.*, 2018, **24**, 585-589.
12 X. Guo, Y. Tian, M. Zhang, Y. Li, R. Wen, X. Li, X. Li, Y. Xue, L. Ma, C. Xia and S. Li, *Chem. Mater.*, 2018, **30**, 2299-2308.
13 Y. Lin, X. Jiang, S. T. Kim, S. B. Alahakoon, X. Hou, Z. Zhang, C. M. Thompson, R. A. Smaldone and C. Ke, *J. Am. Chem. Soc.*, 2017, **139**, 7172-7175.
14 Y. Liao, J. Li and A. Thomas, *ACS Macro Lett.*, 2017, **6**, 1444-1450.
15 J. Li, H. Zhang, L. Zhang, K. Wang, Z. Wang, G. Liu, Y. Zhao and Y. Zeng, *J. Mater. Chem. A.*, 2020, **8**, 9523-9527.
16 X. Guo, Y. Li, M. Zhang, K. Cao, Y. Tian, Y. Qi, S. Li, K. Li, X. Yu and L. Ma, *Angew. Chem. Int. Ed.*, 2020, **59**, 22697-22705.
17 L. He, L. Chen, X. Dong, S. Zhang, M. Zhang, X. Dai, X. Liu, P. Lin, K. Li, C. Chen, T. Pan, F. Ma, J. Chen, M. Yuan, Y. Zhang, L. Chen, R. Zhou, Y. Han, Z. Chai and S. Wang, *Chem*, 2021, **7**, 699-714.
18 S. An, X. Zhu, Y. He, L. Yang, H. Wang, S. Jin, J. Hu and H. Liu, *Ind. Eng. Chem. Res.*, 2019, **58**, 10495-10502.

 This journal is © The Royal Society of Chemistry 20xx

Please do not adjust margins